J Mol Model (2012) 18:3113–3123
DOI 10.1007/s00894-011-1325-8

ORIGINAL PAPER

Hydrogen-bonding interactions in adrenaline–water complexes: DFT and QTAIM studies of structures, properties, and topologies

Hongke Wang · Zhengguo Huang · Tingting Shen · Lingfei Guo

Received: 8 September 2011 / Accepted: 2 December 2011 / Published online: 3 January 2012

Abstract ωB97XD/6-311++G(d,p) calculations were carried out to investigate the hydrogen-bonding interactions between adrenaline (Ad) and water. Six Ad–H_2O complexes possessing various types of hydrogen bonds (H-bonds) were characterized in terms of their geometries, energies, vibrational frequencies, and electron-density topology. Natural bond orbital (NBO) and quantum theory of atoms in molecules (QTAIM) analyses were performed to elucidate the nature of the hydrogen-bonding interactions in these complexes. The intramolecular H-bond between the amino and carboxyl oxygen atom of Ad was retained in most of the complexes, and cooperativity between the intra- and intermolecular H-bonds was present in some of the complexes. H-bonds in which hydroxyls of Ad/water acted as proton donors were stronger than other H-bonds. Both hydrogen-bonding interactions and structural deformation play important roles in the relative stabilities of the complexes. The intramolecular H-bond was broken during the formation of the most stable complex, which indicates that Ad tends to break the intramolecular H-bond and form two new intermolecular H-bonds with the first water molecule.

Keywords Hydrogen bonding interaction · Density functional theory (DFT) · Natural bond orbital (NBO) · Quantum theory of atoms in molecules (QTAIM) · Adrenaline

H. Wang · Z. Huang (✉) · T. Shen · L. Guo
Tianjin Key Laboratory of Structure and Performance for Functional Molecules, College of Chemistry, Tianjin Normal University, Tianjin 300387, People's Republic of China
e-mail: hsxyhzg@126.com

Introduction

Adrenaline (Ad) is a member of the catecholamine series of neurotransmitters. Its chemical structure is shown below:

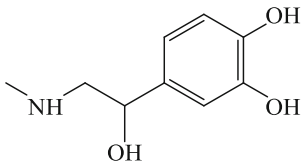

Ad plays an important role in biological systems, since it controls a wide variety of physiological and behavioral processes, mainly through different receptor types. Moreover, the electrochemical behavior of Ad has been the focus of very interesting studies in the past few decades [1–9], and numerous electrochemical methods have been developed to detect Ad. Although the electrochemical response of Ad can be improved by using a modified electrode, the detection of Ad under physiological conditions is still problematic [9–11].

To solve this problem, it is necessary to understand the electrochemical reaction mechanism of Ad, and the crucial factor in this is the structure of Ad. Gas-phase conformations of Ad are well understood [12–20]; for example, they have been studied using ultraviolet spectroscopy (both R2PI and LIF), infrared ion-dip and hole-burning spectroscopy [12, 13], and molecular beam Fourier transform microwave (MB-FTMW) spectroscopy [14]. Moreover, several studies on the conformational landscape of protonated Ad in the gas phase have been reported [15, 17, 18]. However, the conformational landscape of Ad under physiological conditions is more complicated than that in the gas phase, since Ad can form hydrogen bonds (H-bonds) with solvents through

hydroxyl and amino groups, which means that the electrochemical behavior of Ad varies with the particular aqueous environment it is in. An electrochemical study has shown that DMSO has an strong influence on the structure and diffusion kinetics of Ad [21]. Therefore, the above studies on the gas-phase conformations of Ad cannot be to used to accurately elucidate its conformations in aqueous solution. However, it is difficult to identify the supermolecular structures formed during the complexation of Ad with solvent molecules, since their spectral features can be broadened or can overlap with each other. Theoretical tools can be used to investigate the behavior of Ad in aqueous environments, since it is free of the above difficulties. There are some theoretical studies on the conformers of Ad or supermolecular structures formed through complexation of Ad with solvent molecules [20–24]. Alogona reported the conformational landscape of the N-protonated form of adrenaline in the gas phase and in aqueous solution [20]. Yu studied the supermolecular structures that form from protonated Ad and DMSO [22]. Recently, we also carried out some research on protonated Ad/DMSO [23] and noradrenaline/DMSO complexes [24], and the results showed that the solvent has a crucial influence on the conformers of these neurotransmitters in DMSO.

In the work described in this paper, we studied the hydrogen-bonding interactions between Ad and a water molecule via density functional theory (DFT) combined with quantum theory of the atoms in molecules (QTAIM) and natural bond orbital (NBO) analyses. We hope that the results of this study will be helpful in further studies on the microsolvation of Ad, and will increase our understanding of its electrochemical reaction mechanism.

Computational details

All DFT calculations were performed with Gaussian 09 [25] with the default convergence criteria and without any constraint on the geometry. The ωB97XD functional [26] with the 6-311++G(d,p) basis set [27, 28] was used to investigate the electronic structures of the Ad–H_2O systems. The ωB97XD functional includes empirical dispersion and can more accurately treat hydrogen-bonding and van der Waals interactions than conventional DFT. First, the isolated Ad and water monomers were fully optimized; then the complexes were constructed, starting from the most stable Ad and water monomers, and they were also fully optimized at the same level. The harmonic vibrational frequencies were calculated with analytic second derivatives at the same level in order to confirm that the structures were minima and evaluate zero-point vibrational energies (ZPVE). To take into account the effects of basis set superposition error (BSSE), the counterpoise (CP) correction [29] was implemented, thus ensuring that the complexes and monomers were computed with a consistent basis set. The interaction energies were calculated based on the ZPVE and BSSE corrections. In order to analyze the properties of the H-bond interactions in complexes, NBO analysis was carried out using Gaussian 09, and QTAIM analysis was performed using the wavefunctions obtained at the ωB97XD/6-311++G(d,p) level by AIM2000 [30].

Results and discussion

Conformers of Ad have been studied by other groups [12, 15]. In this work, the Ad and water monomers were optimized at the ωB97XD/6-311++G(d,p) level; the molecular graphs are presented in Fig. 1. As shown in Fig. 1, Ad offers several possible proton donor/acceptor sites to form H-bonds. The two phenolic hydroxyls and the hydroxyl linked with the α-carbon are the main H-donor sites of Ad. The methylene of Ad also acts as an H-donor in order to form weak H-bonds in some complexes. The main H-acceptors of Ad are the three oxygen atoms of the hydroxyl groups, and the nitrogen atom usually accepts one proton to form an intramolecular H-bond with the hydroxyl. A water molecule can donate/accept an proton to form an H-bond in which the hydroxyl and the oxygen atom act as H-donor and acceptor, respectively. The benzene ring can also offer a proton to the oxygen atom of H_2O to form a π H-bond.

Structures

In this work, different complexes were taken into account in order to analyze various types of H-bond. Molecular graphs of the optimized Ad–H_2O complexes are shown in Fig. 2, and the structural parameters of the H-bonds are listed in Table 1. No imaginary frequency was found, which verified that all of the optimized complexes were stable. According to QTAIM, the direct proof of the existence of an H-bond can be obtained by considering the bond critical points (BCPs) between the H-donor (X–H) and H-acceptor (Y). The coexistence of multiple H-bonds usually leads to the formation of a ring structure characterized by one ring critical point (RCP), and the union between the RCP and corresponding BCP can be used as a criterion to estimate the structural stability of the H-bond, since a shorter distance means less stability [31]. Of course, as shown in Figs. 1 and 2, there is one RCP at the center of the benzene ring that has no relationship with an H-bond. As shown in Fig. 1, one intramolecular H-bond is formed between the hydroxyl (O1H1) and the nitrogen atom in the Ad monomer, which is characterized by the BCP and the corresponding RCP. This intramolecular $O1H1^A\cdots N^A$ H-bond is retained in all Ad–H_2O complexes except **AW1**. The cleavage of the intramolecular $O1H1^A\cdots N^A$ H-bond in **AW1** indicates that greater structural deformation occurs in **AW1**

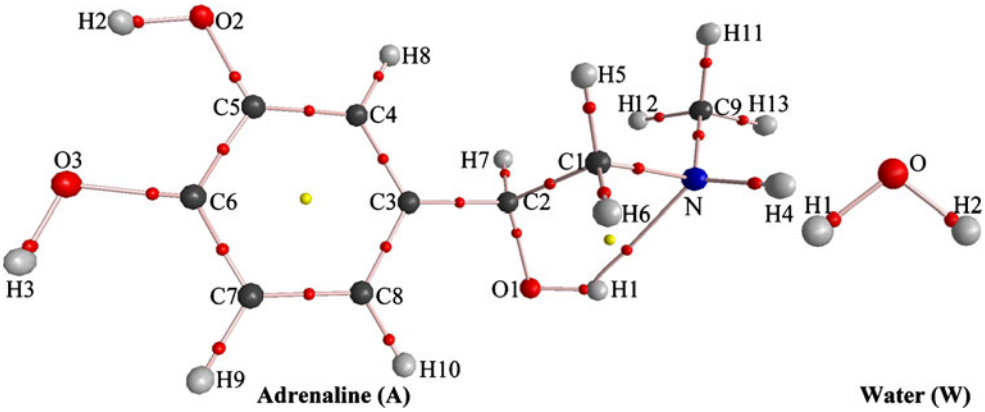

Fig. 1 Molecular graphs of adrenaline (Ad) and water (W) monomers. *Large circles* correspond to attractors: *gray* H, *blue* N, *black* C, *red* O. *Small circles* are attributed to critical points: *red* bond critical point, *yellow* ring critical point (color figure can be viewed in the online issue)

than in the other complexes. From the viewpoint of structure, it is reasonable to form an intramolecular H-bond between two phenolic hydroxyls of Ad [22], and such an intramolecular H-bond can be found in **AW2**, but it is not obtained in QTAIM analyses of the free Ad molecule and other Ad–H_2O complexes. The probable reason for this is that QTAIM is an elegant theory, but one that sometimes gives unrealistic predictions.

As shown in Fig. 2, the oxygen atom of the water moiety accepts two protons from both the hydroxyl and the methylene of Ad simultaneously, to form one bifurcated H-bond in **AW2**. In other Ad–H_2O complexes (**AW1**, **AW3**, **AW4**, and **AW6**), the water moiety acts as an H-donor/H-acceptor to form two intermolecular H-bonds with the Ad moiety simultaneously. **AW5** is a special case; except for the intermolecular H-bonds, there is a tendency to form a π H-bond between the benzene ring of Ad and water moieties when the water is above the benzene ring, since benzene is highly electron withdrawing. However, because the distance between the center of benzene ring and the proton of the hydroxyl of water in **AW5** is about 3.484 Å, this π H-bond is very weak and cannot be confirmed by either QTAIM or NBO analysis. In addition, as shown in Fig. 2, for the $O2H2^{A}\cdots O3^{A}$ H-bond in **AW2**, the BCP almost merges with the corresponding RCP, which indicates that the $O2H2^{A}\cdots O3^{A}$ H-bond is weak and has a tendency to break. Hence, generally speaking, no intramolecular H-bond is formed between the two phenolic hydroxyls of the Ad moiety.

It is well known that H-bond formation is connected with the elongation of the proton-donating X–H bond and the shortening of the H···Y bond (except in the case of so-called blueshifted H-bonds). The shorter the H···Y bond or the longer the X–H bond, the stronger the interaction, and vice versa. As shown in Table 1, the almost unchanged ΔR_{X-H} values and the $R_{H\cdots Y}$ values of >2.5 Å for the H-bonds, taking methylene as the H-donor, indicate that these H-bonds are very weak. The other H-bonds, which have the hydroxyl as the H-donor, have positive ΔR_{X-H} values and are redshifted H-bonds. The largest ΔR_{X-H} (0.027 Å) is found in the $OH1^{W}\cdots N^{A}$ H-bond of **AW1**, which indicates that it is the strongest intermolecular H-bond. It is worth noting that another intermolecular H-bond ($O1H1^{A}\cdots O^{W}$) in **AW1** is also strong, considering its short $R_{H\cdots Y}$ (1.867 Å). However, the ΔR_{X-H} value (0.002 Å) of the intermolecular H-bond ($O1H1^{A}\cdots O^{W}$) in **AW1**, obtained by comparing it with the intramolecular $O1H1^{A}\cdots N^{A}$ H-bond of the Ad monomer, is small. In this case, the strength of the H-bond cannot be estimated based on ΔR_{X-H}. Furthermore, such strong hydrogen-bonding interactions in **AW1** do not mean that it definitely the most stable complex, as the cleavage of the intramolecular $O1H1^{A}\cdots N^{A}$ H-bond results in serious structural deformation, which will be further discussed later.

Since the strength of the H-bond cannot be estimated by ΔR_{X-H} in some cases, an alternative choice is $R_{H\cdots Y}$, and a shorter H···Y bond means a stronger hydrogen-bonding interaction. However, this relationship is only approximate, even when the $R_{H\cdots Y}$ values are for similar species immersed in similar environments; in other words, if the sample of the X–H···Y system is homogeneous. Estimation of H-bond strength directly on the basis of $R_{H\cdots Y}$ is not possible for a heterogeneous sample if the H-bonds differ in the types of H-donors and/or H-acceptors involved. In view of the above difficulties, the H-bond parameter $\delta R_{H\cdots Y}$, which allows interactions to be unified in order to estimate their strength, even when different pairs of atoms are involved, is defined as [32]

$$\delta R_{H\cdots Y} = R_H^{vdW} + R_Y^{vdW} - R_{H\cdots Y} \quad (1)$$

where R_H^{vdW} and R_Y^{vdW} are the van der Waals radii of the H and Y atoms, as given by Bondi [33], respectively; $R_{H\cdots Y}$ is the distance between the H-donor and the H-acceptor. As shown in Table 1, the maximum $\delta R_{H\cdots Y}$ is 0.917 Å, for the intermolecular $O1H1^{W}\cdots N^{A}$ H-bond in **AW1**, which should be the strongest H-bond. Of course, another intermolecular H-bond in **AW1**, $O1H1^{A}\cdots O^{W}$, is also strong because it has a small $\delta R_{H\cdots Y}$ (0.853 Å). It is worth noting that the $\delta R_{H\cdots Y}$ values of the H-bonds in which methylene acts as H-donor in **AW2** and **AW5** are small, which implies that the $R_{H\cdots Y}$ is close to the sum of the van der Waals radii of the H and Y atoms.

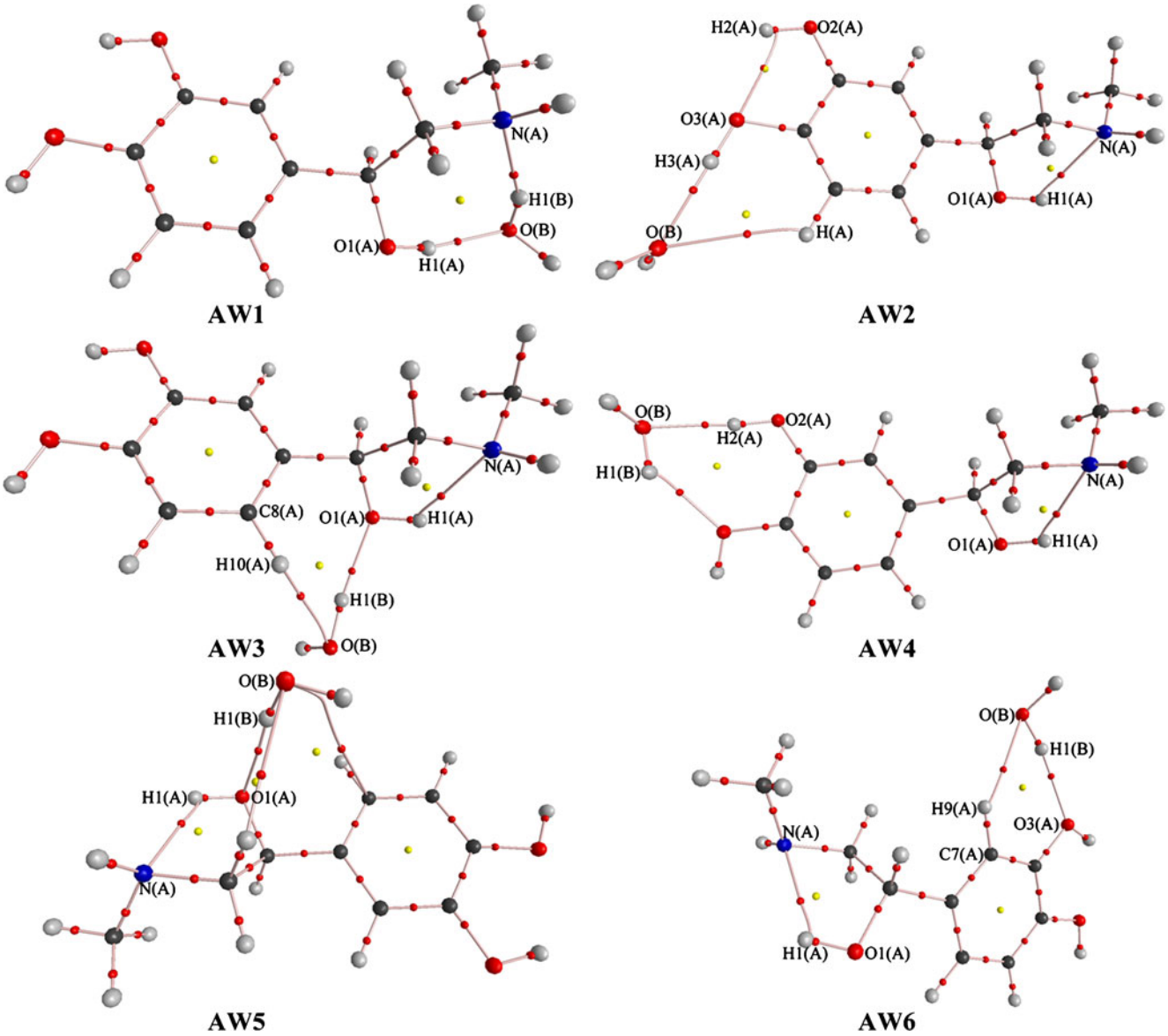

Fig. 2 Molecular graphs of Ad–H_2O complexes. *Large circles* correspond to attractors: *gray* H, *blue* N, *black* C, *red* O. *Small circles* are attributed to critical points: *red* bond critical point, *yellow* ring critical point (color figure can be viewed in the online issue)

Therefore, from a structural viewpoint, the interaction between the methylene and Y atom is very weak and has partial van der Waals character. In addition, both the $\delta R_{H\cdots Y}$ and ΔR_{X-H} values of the intramolecular $O1H1^A\cdots N^A$ H-bond in some Ad–H_2O complexes (**AW2**, **AW4**, and **AW6**) remain almost unchanged, which indicates that the formation of the complex has little influence on the strength of the intramolecular $O1H1^A\cdots N^A$ H-bond, since the intermolecular H-bond is away from the side chain of Ad. However, the $\delta R_{H\cdots Y}$ values of the intramolecular $O1H1^A\cdots N^A$ H-bond in **AW3** and **AW5** are obviously larger than that of the Ad monomer, which indicates that the intramolecular $O1H1^A\cdots N^A$ H-bond is strengthened in these complexes. In other words, certain cooperative effects occur between the intramolecular $O1H1^A\cdots N^A$ H-bond and the intermolecular H-bonds in these complexes.

Vibrational frequencies

The harmonic vibrational frequencies and their shifts for the H-bonds in the Ad–H_2O complexes and monomers calculated at the ωB97XD/6-311++G(d,p) level are listed in Table 2. Redshifts in the X–H stretching vibrational frequency have traditionally been considered one of the main fingerprints of H-bonds, assuming that the formation of an H-bond weakens an X–H single bond. The larger the shift, the stronger the H-bond. However, it is not easy to calculate

Table 1 Structural parameters (bond lengths in Å, angles in degrees) of H-bonds in Ad–H_2O complexes, calculated at the ωB97XD/6-311++G(d,p) level

Complex	H-bond[a]	$R_{X–H}$	$\Delta R_{X–H}$[b]	$R_{H\cdots Y}$	$\delta R_{H\cdots Y}$	∠X–H···Y
AW1	$OH1^{W}\cdots N^{A}$	0.984	0.027	1.833	0.917	160.2
	$O1H1^{A}\cdots O^{W}$	0.969	0.002	1.867	0.853	161.3
AW2	$O3H3^{A}\cdots O^{W}$	0.970	0.012	1.821	0.899	178.6
	$C7H9^{A}\cdots O^{W}$	1.085	−0.001	2.709	0.011	126.5
	$O2H2^{A}\cdots O3^{A}$	0.963	0.001	2.114	0.606	114.5
	$O1H1^{A}\cdots N^{A}$	0.967	0.000	2.129	0.621	120.0
AW3	$OH1^{W}\cdots O1^{A}$	0.970	0.013	1.865	0.855	170.5
	$C8H10^{A}\cdots O^{W}$	1.083	0.001	2.532	0.188	134.0
	$O1H1^{A}\cdots N^{A}$	0.971	0.004	2.076	0.674	121.1
AW4	$O2H2^{A}\cdots O^{W}$	0.973	0.011	1.824	0.896	171.1
	$OH1^{W}\cdots O3^{A}$	0.965	0.008	1.937	0.783	139.1
	$O1H1^{A}\cdots N^{A}$	0.967	0.000	2.126	0.624	120.0
AW5	$OH1^{W}\cdots O1^{A}$	0.967	0.010	2.010	0.710	163.0
	$C1H6^{A}\cdots O^{W}$	1.093	−0.001	2.621	0.099	130.7
	$O1H1^{A}\cdots N^{A}$	0.970	0.003	2.083	0.667	120.0
AW6	$OH1^{W}\cdots O2^{A}$	0.965	0.008	1.952	0.768	162.3
	$C4H8^{A}\cdots O^{W}$	1.086	0.001	2.547	0.173	133.3
	$O1H1^{A}\cdots N^{A}$	0.967	0.000	2.116	0.634	120.3
	$O1H1^{A}\cdots N^{A}$	0.967		2.121	0.629	120.1
Ad	O2H2	0.962				
	O3H3	0.958				
	C4H8	1.085				
	C8H10	1.082				
	C7H9	1.086				
	C1H6	1.094				
Water	OH	0.957				

[a] Superscript "A" denotes adrenaline and superscript "W" denotes H_2O

[b] $\Delta R_{X–H}=R_{X–H}$ (complexes) − $R_{X–H}$(free monomer)

the shift in the X–H stretching vibrational mode if it mixes with other vibrational modes. Strong mixing occurs between the C2H7 and symmetric H5–C1–H6 stretching vibration modes in the free Ad molecule, which are calculated to occur at 3101.5 and 2996.4 cm^{-1}, respectively, so two $\Delta\nu_{X–H}$ values can be obtained for H-bonds involving C1H6 as the H-donor. Similar behavior is also seen for Ad–H_2O complexes. For example, strong mixing occurs between the $O–H1^{W}$ and $O1–H1^{A}$ stretching vibration modes in **AW3**, which leads to different $\Delta\nu_{X–H}$ values for these two vibrational modes with respect to those in free water and Ad molecules, respectively; the $\Delta\nu_{X–H}$ values of the $O–H1^{W}$ stretching vibrational mode are −180.9 and −207.1 cm^{-1}, while they are −42.1 and −68.3 cm^{-1} for the $O1–H1^{A}$ stretching vibrational mode. As shown in Table 2, the largest redshift value of −486.9 cm^{-1} was found for the $OH1^{W}\cdots N^{A}$ H-bond in **AW1**. The $O3H3^{A}\cdots O^{W}$ (**AW2**), $OH1^{W}\cdots O1^{A}$ (**AW3**), and $O2H2^{A}\cdots O^{W}$ (**AW4**) H-bonds have large redshifts of more than −200 cm^{-1}, so the strengths of these H-bonds are regarded as weaker than the $OH1^{W}\cdots N^{A}$ H-bonds in **AW1** and stronger than other redshifted H-bonds. The $O2H2^{A}\cdots O3^{A}$ H-bond in **AW2** has a very small $\Delta\nu_{X–H}$ of −4.5 cm^{-1}, which means that this H-bond is weak, in accord with the above discussion. However, the small $\Delta\nu_{X–H}$ of the intramolecular $O1H1^{A}\cdots N^{A}$ H-bond in Ad–H_2O complexes does not mean that it is also very weak, as it originally existed in the free Ad molecule. Furthermore, the $\Delta\nu_{X–H}$ values of the intramolecular $O1H1^{A}\cdots N^{A}$ H-bond in **AW3** and **AW5** are clearly larger than those in other complexes; such complexes benefit from cooperative effects between the intramolecular $O1H1^{A}\cdots N^{A}$ H-bond and the intermolecular H-bonds.

QTAIM analyses

QTAIM has been shown to be a powerful tool for investigating hydrogen-bonding interactions [32, 34–38]. Topological

Table 2 The X–H stretching vibrational frequencies (strength) of H-bonds in both Ad–H_2O complexes and monomers

Complex	H-bond	ν_{X-H}[a]	$\Delta\nu_{X-H}$
AW1	$OH1^W\cdots N^A$	3415.1(709)	−486.9
	$O1H1^A\cdots O^W$	3703.9(744)	−59.3
AW2	$O3H3^A\cdots O^W$	3710.5(890)	−226.6
	$C7H9^A\cdots O^W$	3230.9(1), 3199.9(1), 3197.6(10)[b]	49.5, 18.5, 16.2[b]
	$O2H2^A\cdots O3^A$	3865.1(107)	−4.5
	$O1H1^A\cdots N^A$	3771.7(138)	8.6
AW3	$OH1^W\cdots O1^A$	3969.7(81, as)	−41.6
		3721.1(275, s)[c], 3694.9(382, s)[c]	−180.9, −207.1[d]
	$C8H10^A\cdots O^W$	3224.2(2)	−7.3
	$O1H1^A\cdots N^A$	3721.1(275)[c], 3694.9(382)[c]	−42.1, −68.3[e]
AW4	$O2H2^A\cdots O^W$	3635.3(820)	−234.4
	$OH1^W\cdots O3^A$	3972.4(127, as), 3808.4(280, s)	−38.9, −93.6
	$O1H1^A\cdots N^A$	3756.4(151)	−6.8
AW5	$OH1^W\cdots O1^A$	3947.8(43, as)[f], 3765.5(188, s)	−63.6[f], −136.5
	$C1H6^A\cdots O^W$	3119.2(5, as), 3012.7(47, s)	17.7, 16.3
	$O1H1^A\cdots N^A$	3711.7(204)	−51.4
AW6	$OH1^W\cdots O2^A$	3973.8(107, as), 3804.8(245, s)	−37.6, −97.2
	$C4H8^A\cdots O^W$	3187.9(2)	−13.0
	$O1H1^A\cdots N^A$	3756.3(155)	−6.9
Ad	O2H2	3869.6(117)	
	O1H1	3763.2(151)	
	O3H3	3937.1(99)	
	C8H10	3231.5(1)	
	C7H9	3181.4(7)	
	C1H6	3101.5(21, as), 2996.4(57, s)[g]	
	C4H8	3200.9(4)	
Water	OH	4011.4(62, as), 3902.0(12, s)	

[a] All frequencies are in cm^{-1} and the strengths are in km mol^{-1}. "as" denotes the asymmetric stretching vibration mode, and "s" denotes the symmetric stretching vibration mode

[b] Mixing occurs among the $C7H9^A$, $C4H8^A$, and $C8H10^A$ stretching vibration modes

[c] Strong mixing occurs between the $OH1^W$ and $O1H1^A$ stretching vibration modes

[d] −41.6 and −180.9 are the $\Delta\nu_{X-H}$ values when compared to the symmetric H–O–H stretching vibration mode of a free water molecule

[e] −42.1 and −68.3 are the $\Delta\nu_{X-H}$ values when compared to the $O1H1^A$ stretching vibration mode of adrenaline

[f] Slight mixing occurs between the $OH1^W$ and $O1H1^A$ stretching vibration modes

[g] Strong mixing occurs between the C2H7 and the symmetric H5–C1–H6 stretching vibration modes

criteria for the existence of hydrogen bonding were proposed by Koch and Popelier [39]. According to these criteria, H-bonds should exhibit relatively high electron density at the H···Y BCP (ρ_b), in the range 0.002–0.034 a.u., and the Laplacian of the electron density at H···Y BCP ($\nabla^2\rho_b$) should be within 0.024–0.139 a.u. [40]. Therefore, both ρ_b and $\nabla^2\rho_b$ at the H···Y BCP are good measures of the strength of the H-bond; moreover, the criteria provide the basis for distinguishing hydrogen-bonding interactions from van der Waals interactions, and have been shown to be valid for both standard and unconventional H-bonds. In addition, other characteristics can be applied to describe the considered BCP as well as the atom–atom interaction. There are well-known relationships that result from the virial theorem between energetic topological parameters and the Laplacian of electron density at the BCP

$$(1/4)\nabla^2\rho_b = 2G_b + V_b \tag{2}$$

$$H_b = G_b + V_b \tag{3}$$

where G_b, V_b, and H_b are the kinetic, potential, and total electron energy densities at the critical point, respectively. G_b is a positive value, and V_b is a negative one. The sign of

H_b depends on which contribution—potential or kinetic—will prevail locally at the BCP. The Laplacian is negative if the modulus of the potential energy is at least twice the kinetic energy, which implies that the interaction has covalent character, so it may involve covalent bonds as well as very strong H-bonds. If the modulus of the potential energy only just outweighs the kinetic energy, the Laplacian is positive but H_b is negative, which implies that the interaction has partial covalent character and involves strong H-bonds [41, 42]. Moreover, the $\nabla^2\rho_b$ at the BCP is small and positive, which is typical of closed-shell interactions. Therefore, the following criterion for H-bond strength was proposed by Popelier [39]: for weak or medium-strength H-bonds, $\nabla^2\rho_b>0$ and $H_b>0$; for strong H-bonds, $\nabla^2\rho_b>0$ and $H_b<0$; for very strong H-bonds, $\nabla^2\rho_b<0$ and $H_b<0$. This classification shows that weak H-bonds eventually merge with (weaker) van der Waals interactions, whereas, at the other end of the continuum, strong H-bonds merge with covalent and polar bonds.

The electronic topological properties at the H···Y BCPs of H-bonds—including the electron density (ρ_b), the Laplacian of the electron density ($\nabla^2\rho_b$), the kinetic energy density (G_b), the potential energy density (V_b), and the total electron energy density (H_b)—for all of the complexes are listed in Table 3. As shown in Table 3, the $OH1^W\cdots N^A$ H-bond in **AW1** is a unique H-bond among all of those in the Ad–H_2O complexes—it lies within the range of strong H-bonds due to its negative H_b value of −0.004051 a.u.; moreover, its ρ_b value of 0.040704 a.u. is beyond the upper limit of the range, so partial covalent character is attributed to it. For the other H-bonds, both ρ_b and $\nabla^2\rho_b$ lie within the ranges proposed by Popelier; moreover, their H_b values are positive, which indicates that these H-bonds are weak or of medium strength. Especially for H-bonds in which methylene acts as the H-donor, both ρ_b and $\nabla^2\rho_b$ are close to the lower limits of the criteria proposed by Popelier, which shows that they are very weak. Another problem is that no direct QTAIM evidence can be found for a π H-bond between the benzene ring and the hydroxyl of the water moiety in **AW5**. Compared with the free Ad molecule, the intramolecular $O1H1^A\cdots N^A$ H-bonds in both **AW3** and **AW5** have larger ρ_b and $\nabla^2\rho_b$ values, while their H_b values are smaller, which indicates that the intramolecular $O1H1^A\cdots N^A$ H-bonds are strengthened by cooperative effects in these complexes. Similar cooperativity is not found in other complexes, since the electron-density topological parameters (ρ_b, $\nabla^2\rho_b$, and H_b) of the intramolecular $O1H1^A\cdots N^A$ H-bonds show only small changes compared to those of the free Ad molecule.

NBO analysis and energy

Generally, a certain amount of charge transfer (CT) from the H-acceptor to the H-donor is one of the characteristics attributed to H-bonds. This CT leads to rearrangement of the electron density within each part of the molecule. According to NBO theory [43], for a typical hydrogen bond, there is a two-electron $n_B \rightarrow \sigma^*_{XH}$ intermolecular donor–acceptor interaction where electron density from the lone pair n_B of the H-acceptor delocalizes into the unfilled σ^*_{XH} antibonding orbital of the H-donor. The $n_B \rightarrow \sigma^*_{XH}$ orbital overlap is characteristic of hydrogen-

Table 3 Electron density (ρ_b), Laplacian of the electron density ($\nabla^2\rho_b$), kinetic energy density (G_b), potential energy density (V_b) and total electron energy density (H_b) in a.u. at BCPs of H-bonds in Ad–H_2O complexes and the Ad monomer, as obtained by QTAIM analysis

Complex	H-bond	ρ_b	$\nabla^2\rho_b$	V_b	G_b	H_b
AW1	$OH1^W\cdots N^A$	0.040704	0.101375	−0.033446	0.029395	−0.004051
	$O1H1^A\cdots O^W$	0.030158	0.106580	−0.024593	0.025619	0.001026
AW2	$O3H3^A\cdots O^W$	0.031128	0.117104	−0.026602	0.027939	0.001337
	$C7H9^A\cdots O^W$	0.006408	0.021981	−0.003906	0.004701	0.000795
	$O2H2^A\cdots O3^A$	0.019155	0.095460	−0.016684	0.020275	0.003590
	$O1H1^A\cdots N^A$	0.023616	0.083449	−0.017713	0.019288	0.001574
AW3	$OH1^W\cdots O1^A$	0.028655	0.107949	−0.023191	0.025089	0.001898
	$C8H10^A\cdots O^W$	0.009162	0.030814	−0.005440	0.006572	0.001132
	$O1H1^A\cdots N^A$	0.026186	0.088946	−0.019877	0.021057	0.001180
AW4	$O2H2^A\cdots O^W$	0.032516	0.111421	−0.027047	0.027451	0.000404
	$OH1^W\cdots O3^A$	0.025203	0.100990	−0.020534	0.022891	0.002357
	$O1H1^A\cdots N^A$	0.023744	0.083780	−0.017821	0.019383	0.001562
AW5	$OH1^W\cdots O1^A$	0.022741	0.077082	−0.016264	0.017767	0.001504
	$C1H6^A\cdots O^W$	0.008141	0.024905	−0.004749	0.005488	0.000738
	$O1H1^A\cdots N^A$	0.026130	0.088705	−0.019845	0.021011	0.001165
AW6	$OH1^W\cdots O2^A$	0.022820	0.091169	−0.017325	0.020059	0.002733
	$C4H8^A\cdots O^W$	0.008441	0.027636	−0.005004	0.005957	0.000952
	$O1H1^A\cdots N^A$	0.024220	0.084768	−0.018213	0.019703	0.001489
Ad	$O1H1^A\cdots N^A$	0.024040	0.084410	−0.018070	0.019586	0.001516

Table 4 The second-order perturbation energies $E(2)$ (in kcal·mol^{-1}) of the H-bonds in Ad–H_2O complexes and the AD monomer, as obtained by NBO analysis

Complex	H-bond	$E(2)$[a]	Complex	H-bond	$E(2)$[a]
AW1	$OH1^{W}\cdots N^{A}$	21.55	AW4	$O2H2^{A}\cdots O^{W}$	0.26(16.82)
	$O1H1^{A}\cdots O^{W}$	0.11(13.58)		$OH1^{W}\cdots O3^{A}$	5.05(0.89)
AW2	$O3H3^{A}\cdots O^{W}$	15.08(0.06)		$O1H1^{A}\cdots N^{A}$	4.91
	$C7H9^{A}\cdots O^{W}$	0.44(0.1)	AW5	$OH1^{W}\cdots O1^{A}$	0.67(6.81)
	$O2H2^{A}\cdots O3^{A}$	1.5		$C1H6^{A}\cdots O^{W}$	0.88
	$O1H1^{A}\cdots N^{A}$	4.85		$O1H1^{A}\cdots N^{A}$	6.46
AW3	$OH1^{W}\cdots O1^{A}$	3.89(7.7)	AW6	$OH1^{W}\cdots O2^{A}$	5.49(0.44)
	$C8H10^{A}\cdots O^{W}$	0.07(0.87)		$C4H8^{A}\cdots O^{W}$	0.07(1.19)
	$O1H1^{A}\cdots N^{A}$	6.56		$O1H1^{A}\cdots N^{A}$	5.19
Ad	$O1H1^{A}\cdots N^{A}$	5.07			

[a] The values not in parentheses refer to H-bond formation via the O *sp* hybrid; those in parentheses refer to H-bond formation via the O *p* hybrid. The lone pair on the N atom mainly has *p* character. See discussion in the text

bonding interactions. The formation of the hydrogen bond leads to an increase in the occupancy of the σ^*_{XH} antibonding orbital and hence a weakening and lengthening of the X–H bond. This leads to the redshifted ν_{X-H} stretching frequency. Therefore, electron delocalization or CT effects between n_B and σ^*_{XH}can be estimated by second-order perturbation theory:

$$E(2) = -2\frac{\langle n_B|F|\sigma^*_{XH}\rangle^2}{\varepsilon(\sigma^*_{XH}) - \varepsilon(n_B)} \quad (4)$$

where $\langle n_B|F|\sigma^*_{XH}\rangle$ is the Fock matrix element between the n_B and σ^*_{XH} orbitals, $\varepsilon(\sigma^*_{XH}) - \varepsilon(n_B)$ is the orbital energy difference (the difference in the diagonal Fock matrix elements). Therefore, the CT and the corresponding lowering of energy are attributed to hydrogen bonding interactions, and the second-perturbation energies $E(2)$ lowering is responsible for the orbital interaction of H-bond, the larger $E(2)$ values correspond to stronger CT interaction occurred in the H-bond.

The results of the NBO analysis are listed in Table 4. From Table 4, the atom that most commonly acts as the H-acceptor in the H-bond is O, and it is clear that there are two "branches" of H-acceptor O atoms: one has *sp* hybrid characteristics and the other has *p* hybrid characteristics; these each yield a different $E(2)$ value. The O atom involved as H-acceptor in **AW2** ($O2H2^{A}$...$O3^{A}$) and **AW5** ($C1H6^{A}$...OW) has one *sp* branch, while the O atom in other H-bonds has one *sp* branch and one p branch. When the N atom is involved as the H-acceptor, it also shows *sp* characteristics. The $E(2)$ values of the intramolecular $O1H1^{A}\cdots N^{A}$ H-bond in some complexes (**AW3** and **AW5**) are significantly larger than that that of the Ad monomer, which confirms the existence of cooperativity between the intra- and intermolecular H-bonds. Without such cooperativity, the $E(2)$ value of the intramolecular $O1H1^{A}\cdots N^{A}$ H-bond in other Ad–H_2O complexes barely changes compared to that of the Ad monomer. The largest $E(2)$ value (21.55 kcal·mol^{-1}) was found for the $OH1^{W}\cdots N^{A}$ H-bond of **AW1**, which indicates that the strongest CT interaction is responsible for the H-bond. The $O2H2^{A}\cdots O3^{A}$ H-bond of **AW2** is the weakest intermolecular H-bond involving a hydroxyl group, because it has the smallest $E(2)$ value of 1.5 kcal·mol^{-1}. In addition, the $E(2)$ values of the H-bonds with hydroxyl as the H-donor are larger than those of the H-bonds with methylene as the H-donor, which is consistent with the above discussion.

Table 5 Total energies (E), preparation energies (ΔE_{prep}), charge-transfer energies (ΔE_{CT}), non-charge-transfer energies (ΔE_{NCT}), interaction energies (ΔE_{int}), and binding energies (ΔE) of the Ad–H_2O complexes, calculated at the ωB97XD/6-311++G(d,p) level[a]

Complex	E[b]	ΔE_{int}	ΔE_{CT}	ΔE_{NCT}	ΔE_{prep}	ΔE
AW1	−707.379025	−6.08	−35.24	29.16	4.07	−2.00
AW2	−707.378390	−5.68	−15.68	10.00	0.20	−5.48
AW3	−707.377329	−5.01	−12.53	7.52	0.76	−4.26
AW4	−707.376404	−4.43	−23.02	18.59	2.00	−2.43
AW5	−707.376114	−4.25	−8.36	4.11	1.03	−3.21
AW6	−707.375597	−3.92	−7.19	3.27	0.18	−3.74
Ad	−630.958683					
Water	−76.410660					

[a] All energies are in kcal·mol^{-1}, except for the total energy (which is in Hartrees)

[b] The total energies of the complexes include ZPVE and BSSE corrections, while the energies of the monomers (Ad and H_2O) include ZPVE correction

To explore the nature of the hydrogen-bonding interaction, an energy decomposition analysis is required. According to NBO theory, the decomposition of the interaction energy (ΔE_{int}) can be presented as

$$\Delta E_{int} = E_{AW} - E_A - E_W = \Delta E_{NCT} + \Delta E_{CT} \quad (5)$$

where E_{AW} is the energy of the Ad–H_2O complex (**AW**), E_A and E_W are the energies of the most stable monomers, and ΔE_{CT} and ΔE_{NCT} are the CT and non-CT energies, respectively. ΔE_{CT} accounts for the orbital and polarization interactions, while ΔE_{NCT} relates to the classical electrostatic and Pauli steric repulsion interactions. In the NBO scheme, the CT interaction is linked to the shift in occupancy from the manifold of filled orbitals of one monomer to the unfilled orbitals of the other. As proposed by Reed et al. [43], ΔE_{CT} values between the Ad and H_2O moieties in the complexes can be obtained from by summing the $E(2)$ values of the intermolecular H-bonds; the negative of this sum is ΔE_{CT}. In the NBO scheme, ΔE_{CT} is negative because it is evaluated as the variational energy lowering due to the expansion of the variational space on each monomer to include unfilled orbitals on the other monomer. ΔE_{NCT} terms with positive values arise from exclusive repulsion and electrostatic (induction and polarization) interactions, and can be obtained from Eq. 5. Based on NBO theory, the binding energy (ΔE) of the **AW** complex is also influenced by both the deformation of the monomers (Ad and water) and ΔE_{int}, and ΔE can be decomposed into

$$\Delta E = \Delta E_{prep} + \Delta E_{int} \quad (6)$$

where ΔE_{prep} is the preparation energy

$$\Delta E_{prep} = E_{AW} - E_{A(W)} - E_{W(A)} \quad (7)$$

Here, $E_{A(W)}$ (or $E_{W(A)}$) is the energy of the Ad (or water) monomer when all the nucleus structure units of water (or Ad) are considered as puppet atoms of carrying empty orbital. ΔE_{prep} is the amount of energy required to deform the separate moieties from their free monomer structures to the geometries that they acquire in the pair complex; ΔE_{int} represents the actual energy change when the prepared moieties are combined to form the pair complex. ΔE_{prep} is positive because the structural deformation causes the molecular energy to jump to a higher energy level, while ΔE_{int} is negative unless the complex is less stable than the monomers. The results of the energy decomposition of the interaction based on the NBO approach are listed in Table 5.

As shown in Table 5, the largest ΔE_{CT} of −35.24 kcal·mol^{-1} is responsible for the strong CT effect that occurs in **AW1**. A strong non-CT effect (ΔE_{NCT}=29.16 kcal·mol^{-1}) also occurs in **AW1**, which results in the strongest interaction energy of ΔE_{int} of −6.08 kcal·mol^{-1}, indicating that **AW1** is the most stable complex. However, cleavage of the intramolecular O1H1^{A}···N^{A} H-bond in **AW1** results in serious structural deformation and counteracts this strong hydrogen bonding to a large extent, as can be seen from the largest ΔE_{prep} of 4.07 kcal·mol^{-1}. Therefore, the binding energy (ΔE=−2.00 kcal·mol^{-1}) of **AW1** is the smallest among all the Ad–H_2O complexes, which suggests that replacing the intramolecular O1H1^{A}···N^{A} H-bond with two intermolecular ones does not favor the binding energy of **AW1**. Similar to **AW1**, **AW4** has the second strongest CT effect (ΔE_{CT}=−23.02 kcal·mol^{-1}) among the Ad–H_2O complexes, but this is countered by the second largest ΔE_{prep} of 2.00 kcal·mol^{-1} to some degree. The slight structural deformation of **AW2**, which has the smallest ΔE_{prep} (0.20 kcal·mol^{-1}) and a strong CT effect (ΔE_{int}=−15.68 kcal·mol^{-1}), can be attributed to the smallest binding energy (ΔE=−5.48 kcal·mol^{-1}). All other complexes have ΔE_{prep} values of less than about 1.0 kcal·mol^{-1}. In conclusion, the order of ΔE_{int} is not consistent with that of the binding energy (ΔE), since both hydrogen-bonding interactions and structural deformation are the two most important aspects of the stability of the complexes.

Conclusions

In this work, we studied the geometries, energies, and IR characteristics of the H-bonds of Ad–H_2O complexes at the ωB97XD/6-311++G(d,p) level. The intramolecular O1H1^{A}···N^{A} H-bond is retained in all complexes except for **AW1**. Cooperativity between the intra- and intermolecular H-bonds exists in **AW3** and **AW5**, while no such cooperativity is found in other Ad–H_2O complexes, since the intermolecular H-bond is away from the side chain of Ad. Both hydrogen-bonding interactions and structural deformation play important roles in the relative stabilities of the complexes. Although its strong CT effect is counteracted by its serious structural deformation to a great extent, **AW1** is the most stable complex, which implies that Ad tends to break the intramolecular O1H1^{A}···N^{A} H-bond and form two new intermolecular H-bonds with the first water molecule. In conclusion, the various hydrogen-bonding motifs that have been shown to occur in the studied complexes may aid our understanding of the hydrogen-bonding interactions between Ad and other small organic molecules.

Acknowledgments This work is supported by Tianjin Science and Technology Development Fund Projects in Colleges and Universities (no. 20080504).

References

1. Song YZ (2007) Theoretical study on the electrochemical behavior of norepinephrine at Nafion multi-walled carbon nanotubes modified pyrolytic graphite electrode. Spectrochem Acta Pt A 67: 1169–1177

2. Baron R, Zayats M, Willner I (2005) Dopamine-, L-DOPA-, adrenaline-, and noradrenaline-induced growth of Au nanoparticles: assays for the detection of neurotransmitters and of tyrosinase activity. Anal Chem 77:1566–1571
3. Chen SM, Peng KT (2003) The electrochemical properties of dopamine, epinephrine, norepinephrine, and their electrocatalytic reactions on cobalt(II) hexacyanoferrate films. J Electroanal Chem 547:179–189
4. Perati PR, Cheng J, Jandik P, Hanko VP (2010) Disposable carbon electrodes for liquid chromatographic detection of catecholamines in blood plasma samples. Electroanalysis 22:325–332
5. Chen W, Lin XH, Luo HB, Huang LY (2005) Electrocatalytic oxidation and determination of norepinephrine at poly(cresol red) modified glassy carbon electrode. Electroanalysis 17:941–945
6. Dong H, Wang SH, Liu AH, Galligan JJ, Swain GM (2009) Drug effects on the electrochemical detection of norepinephrine with carbon fiber and diamond microelectrodes. J Electroanal Chem 632:20–29
7. Luczak T (2009) Electroanalysis of norepinephrine at bare gold electrode pure and modified with gold nanoparticles and S-functionalized self-assembled layers in aqueous solution. Electroanalysis 12:1539–1549
8. Seol H, Jeong H, Jeon S (2009) A selective determination of norepinephrine on the glassy carbon electrode modified with poly(ethylenedioxypyrrole dicarboxylic acid) nanofibers. J Solid State Electrochem 13:1881–1887
9. Yao H, Li SG, Tang YH, Chen Y, Chen YZ, Lin XH (2009) Selective oxidation of serotonin and norepinephrine over eriochrome cyanine R film modified glassy carbon electrode. Electrochim Acta 54:4607–4612
10. Zare HR, Nasirizadeh N (2010) Simultaneous determination of ascorbic acid, adrenaline and uric acid at a hematoxylin multiwall carbon nanotube modified glassy carbon electrode. Sensors Actuator B Chem 143:666–672
11. Viry L, Derre A, Poulin P, Kuhn A (2010) Discrimination of dopamine and ascorbic acid using carbon nanotube fiber microelectrodes. Phys Chem Chem Phys 12:9993–9995
12. Carcabal P, Snoek LC, Van Mourik T (2005) A computational and spectroscopic study of the gas-phase conformers of adrenaline. Mol Phys 103:1633–1639
13. Butz P, Kroemer RT, Macleod NA, Simons JP (2001) Conformational preferences of neurotransmitters: ephedrine and its diastereoisomer, pseudoephedrine. J Phys Chem A 105:544–551
14. Alonso JL, Sanz ME, Lopez JC, Cortijo V (2009) Conformational behavior of norephedrine, ephedrine, and pseudoephedrine. J Am Chem Soc 131:4320–4326
15. Butz P, Kroemer RT, Macleod NA, Simons JP (2002) Hydration of neurotransmitters: a spectroscopic and computational study of ephedrine and its diastereoisomer pseudoephedrine. Phys Chem Chem Phys 4:3566–3574
16. Snoek LC, van Mourik T, Carcabal P, Simons JP (2003) Neurotransmitters in the gas phase: hydrated noradrenaline. Phys Chem Chem Phys 5:4519–4526
17. van Mourik T (2004) The shape of neurotransmitters in the gas phase: a theoretical study of adrenaline, pseudoadrenaline, and hydrated adrenaline. Phys Chem Chem Phys 6:2827–2837
18. Macleod NA, Simons JP (2006) Infrared photodissociation spectroscopy of protonated neurotransmitters in the gas phase. Mol Phys 104:3317–3328
19. Vaden TD, de Boer T, MacLeod NA, Marzluff EM, Simons JP, Snoek LC (2007) Infrared spectroscopy and structure of photochemically protonated biomolecules in the gas phase: a noradrenaline analogue, lysine and alanyl alanine. Phys Chem Chem Phys 9:2549–2555
20. Alagona G, Ghio C (2007) Competitive H-bonds in vacuo and in aqueous solution for N-protonated adrenaline and its monohydrated complexes. J Mol Struct (THEOCHEM) 811:223–240
21. Yu ZY, Liu T, Guo DJ, Liu YJ, Liu CB (2010) Experimental and theoretical evaluation on the microenvironmental effect of dimethyl sulfoxide on adrenaline in acid aqueous solution. J Mol Struct 984:402–408
22. Yu ZY, Guo DJ, Wang HQ (2004) Theoretical study on the hydrogen bond interaction between adrenaline and dimethyl sulphoxide. Chin J Chem Phys 17:149–154
23. Huang ZG, Dai YM, Yu L (2010) Density functional theory and topological analysis on the hydrogen bonding interactions in N-protonated adrenaline-DMSO complexes. Struct Chem 21:863–872
24. Huang ZG, Dai YM, Yu L, Wang HK (2011) Hydrogen bonding interactions in noradrenaline-DMSO complexes: DFT and QTAIM studies of structure, properties and topology. J Mol Model 17:2609–2621
25. Frisch MJ, Trucks GW, Schlegel HB, Scuseria GE, Robb MA, Cheeseman JR, Scalmani G, Barone V, Mennucci B, Petersson GA, Nakatsuji H, Caricato M, Li X, Hratchian HP, Izmaylov AF, Bloino J, Zheng G, Sonnenberg JL, Hada M, Ehara M, Toyota K, Fukuda R, Hasegawa J, Ishida M, Nakajima T, Honda Y, Kitao O, Nakai H, Vreven T, Montgomery JA Jr, Peralta JE, Ogliaro F, Bearpark M, Heyd JJ, Brothers E, Kudin KN, Staroverov VN, Kobayashi R, Normand J, Raghavachari K, Rendell A, Burant JC, Iyengar SS, Tomasi J, Cossi M, Rega N, Millam JM, Klene M, Knox JE, Cross JB, Bakken V, Adamo C, Jaramillo J, Gomperts R, Stratmann RE, Yazyev O, Austin AJ, Cammi R, Pomelli C, Ochterski JW, Martin RL, Morokuma K, Zakrzewski VG, Voth GA, Salvador P, Dannenberg JJ, Dapprich S, Daniels AD, Farkas Ö, Foresman JB, Ortiz JV, Cioslowski J, Fox DJ (2009) Gaussian 09. Gaussian Inc., Wallingford CT
26. Chai JD, Head-Gordon M (2008) Long-range corrected hybrid density functionals with damped atom–atom dispersion corrections. Phys Chem Chem Phys 10:6615–6620
27. Krishnan R, Binkley JS, Seeger R, Pople JA (1980) Self-consistent molecular orbital methods. XX. A basis set for correlated wave functions. J Chem Phys 72:650–654
28. McLean AD, Chandler GS (1980) Contracted Gaussian basis sets for molecular calculations. I. Second row atoms, $Z=11$–8. J Chem Phys 72:5639–5648
29. Boys SF, Bernardi F (1970) The calculation of small molecular interactions by the differences of separate total energies. Some procedures with reduced errors. Mol Phys 19:553–566
30. Biegler-König F, Schönbohm J (2000) AIM2000, 10th edn. University of Applied Sciences, Bielefeld
31. Popelier PLA (1998) Characterization of a dihydrogen bond on the basis of the electron density. J Phys Chem A 102:1873–1878
32. Tian SX (2004) Quantum chemistry studies of glycine–H_2O_2 complexes. J Phys Chem B 108:20388–20396
33. Bondi A (1964) van der Waals volumes and radii. J Phys Chem 68:441–451
34. Galvez O, Gomez PC, Pacios LF (2003) Variation with the intermolecular distance of properties dependent on the electron density in cyclic dimers with two hydrogen bonds. J Chem Phys 118:4878–4895
35. Miao R, Jin C, Yang GS, Hong J, Zhao CM, Zhu LG (2005) Comprehensive density functional theory study on serine and related ions in gas phase: conformations, gas phase basicities, and acidities. J Phys Chem A 109:2340–2349
36. Nozad AG, Meftah S, Ghasemi MH, Kiyani RA, Aghazadeh M (2009) Investigation of intermolecular hydrogen bond interactions in crystalline L-cysteine by DFT calculations of the oxygen-17, nitrogen-14, and hydrogen-2 EFG tensors and AIM analysis. Biophys Chem 141:49–58

37. Parreira RLT, Valdes H, Galembeck SE (2006) Computational study of formamide–water complexes using the SAPT and AIM methods. Chem Phys 331:96–110
38. Zhou HW, Lai WP, Zhang ZQ, Li WK, Cheung HY (2009) Computational study on the molecular inclusion of andrographolide by cyclodextrin. J Comput Aided Mol Des 23:153–162
39. Koch U, Popelier PLA (1995) Characterization of C–H–O hydrogen bonds on the basis of the charge density. J Phys Chem 99:9747–9754
40. Popelier PLA (2000) Atoms in molecules: an introduction. Prentice Hall, London
41. Arnold WD, Oldfield E (2000) The chemical nature of hydrogen bonding in proteins via NMR: J-couplings, chemical shifts, and AIM theory. J Am Chem Soc 122:12835–12841
42. Pacios LF (2004) Topological descriptors of the electron density and the electron localization function in hydrogen bond dimers at short intermonomer distances. J Phys Chem A 108:1177–1188
43. Reed AE, Weinhold F, Curtiss LA, Pochatko DJ (1986) Natural bond orbital analysis of molecular interactions: theoretical studies of binary complexes of HF, H_2O, NH_3, N_2, O_2, F_2, CO, and CO_2 with HF, H_2O, and NH_3. J Chem Phys 84:5687–5705